

ORIGINAL ARTICLE OPEN ACCESS

Numerical Investigations of the Aerothermal Performance of Modern Turbine Blade Tip Geometries at Design and Off-Design Conditions and Under Stationary and Moving Shroud

Kheir-Eddine Arrif¹ | Zakaria Mansouri² | Salaheddine Azzouz³

¹Mechanics of Materials and Plant Maintenance Research Laboratory (LR3MI), Mechanical Engineering Department, Faculty of Engineering, Badji Mokhtar - Annaba University, Annaba, Algeria | ²Department of Engineering, Nottingham Trent University, Nottingham, UK | ³Laboratory of Energy Systems Technologies (LTSE), Department of Process Engineering and Energetics, National Higher School of Technology and Engineering, Annaba, Algeria

Correspondence: Zakaria Mansouri (zak.mansouri@ntu.ac.uk)

Received: 17 November 2024 | **Revised:** 5 March 2025 | **Accepted:** 26 March 2025

Keywords: mixing losses | shelf tips | squealer tip | thermal load | tip leakage flow | turbine blade

ABSTRACT

High-pressure turbine blade tips operate under extreme thermal stress, generating significant aerodynamic losses that must be continually optimized to improve engine efficiency and durability. This study uses computational fluid dynamics (CFD) to investigate the aerodynamic and thermal behavior of advanced turbine blade tip configurations, specifically GE's vertical and inclined shelf tips, under both design and off-design transonic conditions. Conventional designs, such as flat and squealer tips, were also analyzed for comparison. Shroud motion effects were included to simulate turbine stage rotation. The simulations are performed by solving the three-dimensional, steady and turbulent form of the Reynolds-Averaged Navier-Stokes (RANS) equations using the Ansys-CFX. A two-equation turbulence model, Shear stress transport (SST) with Gamma-Theta transition formulation is used. CFD results showed strong alignment with experimental data, validated through isentropic Mach number and heat flux measurements. The results revealed that cavity-based designs (squealer and shelf tips) exhibited complex secondary flow structures within the tip cavity, including the formation of suction-side and pressure-side cavity vortices (SSCV and PSCV), which contribute to the tip leakage vortex (TLV) and associated aerodynamic losses. The vertical shelf tip demonstrated the lowest leakage rate in both stationary and moving conditions, attributed to its narrow cavity width and reduced PSCV size, while the inclined shelf exhibited the highest heat transfer coefficient (HTC), beneficial for cooling applications but paired with higher leakage and mixing losses. Notably, these findings differ from previous results on GE's shelf tip, where the inclined shelf had the lowest leakage rate.

1 | Introduction

With the continuous developments in recent technologies of gas turbines, the inlet temperature of the turbine is considerably increased to improve gas turbine aerothermal and mechanical performances (i.e., thermal efficiency, output, thrust-to-weight ratio, etc.). However, the maximum inlet temperature of the

turbine is still limited due to the melting point of the alloys used for blade manufacturing. The rotor blade tip is one of the most vulnerable parts of the turbine components. It allows blade rotation since it has a gap between it and the casing. A portion of the mainstream leaks through this gap and it is called tip leakage flow. This flow increases the aerothermal load on and around the rotor blade tip surface, which causes blade failure

This is an open access article under the terms of the [Creative Commons Attribution](https://creativecommons.org/licenses/by/4.0/) License, which permits use, distribution and reproduction in any medium, provided the original work is properly cited.

© 2025 The Author(s). *Heat Transfer* published by Wiley Periodicals LLC.

after many hours of continuous service. The tip leakage flow also generates a secondary flow, namely tip leakage, that generates undesirable aerodynamic losses.

Several research studies have been conducted on turbine blade tips to identify their aerothermal behaviors, characteristics, and performances [1–11]. Bunker [1–3], conducted and reviewed numerous studies on rotor blade tips. He revealed design criteria for rotor tip geometries considering various design parameters, such as tip gap height, tip shape, and cooling film schemes. Flow behavior and heat transfer on conventional design flat tips have been widely investigated and understood in both early [4, 5] and new studies [6, 7]. The effects of the relative motion between the rotor blade tip and the casing have also been investigated in [8–11]. It was shown that relative motion has a considerable effect on the thermal load distribution of linear cascades tip surface, such as the heat transfer coefficient (HTC). It also affects the strength of the tip leakage vortex (TLV) and alters the aerodynamic loss.

A tip cavity, which is known as a squealer tip, was introduced to reduce the intensity of secondary vortices near the rotor tip [12, 13]. The cavity is enclosed by a rim that takes the exact shape of the blade's pressure and suction surfaces. A squealer tip allows a smaller tip clearance without the risk of a catastrophic failure in case the tip rubs against the shroud during turbine operation. The smaller tip gap (also called clearance) reduces the flow leakage between the blade and casing, resulting in smaller losses and higher heat transfer. Key and Arts [9] conducted experimental measurements of static pressure on turbine blade flat and squealer tips and oil visualization to investigate the flow field on the tip surface. They found that a squealer tip significantly reduces the aerodynamic losses compared to a flat tip. Several studies of aerothermal characteristics of squealer tips have been performed, investigating tip gap height, cavity depth, cavity width, and rim geometry. El-Ghandour et al. [14] investigated the depth of the squealer tip cavity. As the depth of the cavity increases, the vortex formed inside it becomes stronger and this reduces the mass flow rate of the leakage flow. Mischo et al. [15] studied numerically the depth, width, and location of the squealer tip cavity. They found that by reducing the width of the cavity, a recirculation zone was formed, which led to a decrease in the leakage flow by 25% with a decrease in the thermal load.

Novel blade tip geometries have been proposed and investigated recently in the literature based on the modification of the conventional squealer tip [16–24]. Kim et al. [16] investigated the aerothermal performance of six different partial squealer tip configurations by using CFD. They reported that the partial squealer tip having 75% rim on both pressure and suction surfaces has led to the minimum aerodynamic losses. Jiang et al. [17] simulated three different squealer winglet tips and presented their aerothermal data. The results revealed that the suction side (SS) squealer winglet reduces the aerodynamic losses by 8.5% compared to the conventional squealer tip. Lomakin et al. [18] compared turbine stage efficiencies of nine various squealer tip configurations with different cutback and rim inclinations. They found that the squealer tip with both cutback and inclination is more efficient by 0.5% compared to the flat tip. Moreover, a honeycomb structure can produce

around a 10.5% reduction in leakage flow compared to a flat tip due to the induced flow resistance, as discovered by Yunfeng et al. [19].

Other studies of squealer tips with winglet geometry were performed by Zhou and Zhong [20, 21] to determine tip heat transfer according to winglet geometries. They provided useful guidelines for designing efficient winglet squealer tips. Lee et al. [22] conducted wind tunnel experiments and used kerosene to visualize the flow surface on the winglet tip configuration. The authors stated that the secondary flows are strongly affected by the winglet extension. For example, the TLV strengthens, whereas the passage vortex weakens as the length of the winglet increases. Moreover, GE Aircraft Engines [23, 24] has designed and patented an efficient tip configuration, which is currently being used in the new generation of turbofan engines. The blade tip consists of a shifted pressure side (PS) rim toward the blade camber line, which is known as a “shelf squealer tip.” Prakash et al. [24] briefly analyzed this configuration using CFD. They revealed that an inclined shelf configuration effectively reduces the leakage flow rate compared to both a vertical shelf tip and a conventional squealer tip. Whereas the vertical shelf tip configuration has the best turbine efficiency.

The aerodynamics of GE's shelf tip, a critical component in modern turbofan engines, remains poorly understood, and its thermal characteristics have yet to be systematically explored in the existing body of literature. As the shelf tip design is integral to the performance of new-generation turbofan engines, such as the GENx series, it represents a significant advancement in aerospace engineering and aligns with emerging trends in the pursuit of enhanced efficiency and reduced environmental impact. Despite its importance, the lack of comprehensive studies on this component has left a notable gap in the understanding of its aerodynamic behavior and thermal dynamics. Thus, this study aims to fill this specific gap in the existing literature by deeply investigating the influence of the shelf squealer tip on both the aerodynamic performance (i.e., aerodynamic losses, secondary flows, and tip leakage) and the thermal characteristics (i.e., heat transfer), of a high-speed turbine blade operating in a transonic regime. The analysis will examine the shelf squealer tip under both design (nominal exit Mach number) and off-design (supersonic Mach number) conditions, which are critical for rotor tip design, as off-design scenarios represent engine conditions during take-off and climb. To this end, both vertical and inclined shelf squealer tips were designed and will be compared with a flat tip and conventional squealer tip configurations. Aerodynamic performance will be assessed through parameters such as total pressure losses, tip leakage flow rate, secondary flow patterns visualized with 3D streamlines, and surface flows visualized with 2D streamlines. Thermal performance will be evaluated using contour and plot of the wall HTC. Additionally, the shelf tip will be tested in both stationary conditions, to simulate laboratory experiments, and in moving conditions (shroud motion), to replicate turbine stage rotation.

The rest of the paper is structured as follows. Section 2 presents the adopted turbine rotor blade airfoil with the different tip configurations (flat, squealer, vertical shelf, and inclined shelf). Section 3 discusses the numerical method used, including the

solver, turbulence model, boundary conditions, and mesh sensitivity study. In Section 4 validation of the numerical method with the experimental measurements from the literature is provided. Section 5 showcases the findings of the aerothermal performance of the four proposed tips at different conditions, including design, off-design, stationary, and moving cases. Finally, concluding remarks are provided in section 6.

2 | Blade Cascade Configuration

Figure 1 shows the geometry of the examined 2D rotor cascade. The 2D airfoil was designed for high-pressure (HP) turbines of high bypass ratio turbofan engines. It is a high-speed airfoil and has a design inflow angle $\alpha = 27.43^\circ$. It is characterized by a span $H = 50$ mm, a chord $C = 43.63$ mm, and a pitch $\sigma = 36.79$ mm. The 2D airfoil of this rotor has been subject to multiple experimental assessments by Nicholson et al. [25] at design and off-design conditions. The authors performed the investigations to understand the importance of some parameters, such as Reynolds number (Re), isentropic Mach number (M_{is}), and free-stream turbulence (I) on the surface aerodynamic and thermal loads. In the present study, one design and one off-design conditions were selected from Nicholson et al. [25], as shown in Table 1. Both cases have the same Re which is based on the axial blade chord at the cascade exit, inlet turbulence intensity (I), and tip gap height (g) based on the blade height. However, the off-design condition ($M_{is} = 1.1$) is characterized by a higher isentropic Mach number and a correspondingly lower pressure ratio (PR). This specific case was selected because it represents the highest isentropic Mach number examined in Nicholson et al. [25], which corresponds to a high-thrust operating condition of a turbofan engine, such as during the take-off phase. Such a condition is particularly relevant for investigating the aerodynamic and thermal performance of the shelf tip, as it subjects the component to

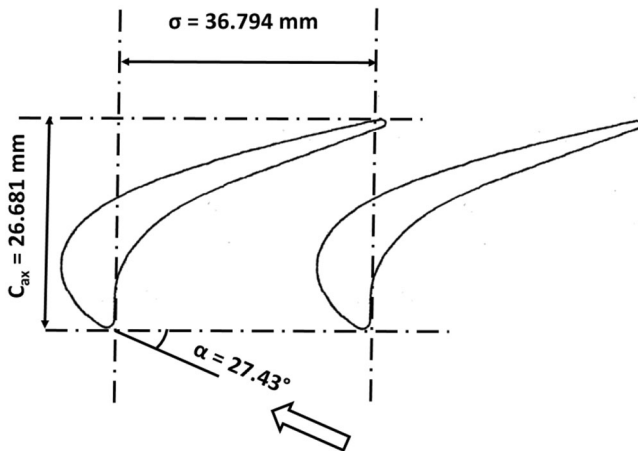


FIGURE 1 | Rotor blade schematic diagram and nomenclature.

TABLE 1 | Investigated operating conditions.

Case	M_{is}	Re	P_0 (bar)	M_{inlet}	PR	I (%)	g (%)	Stationary shroud	Moving shroud
Design	0.78	1.11×10^6	3.2	0.18	0.669	4	2	x	x
Off-design	1.1	1.11×10^6	3.2	0.2	0.468	4	2	x	—

extreme flow velocities and thermal loads. The off-design case will be compared with the design case ($M_{is} = 0.78$), which typically corresponds to the cruise phase of the flight. Thus, the study will highlight the differences in shelf tip performance under these two conditions.

Four blade tip configurations were designed for this study, as shown in Figure 2. The first case (Figure 2a) is a flat tip similar to the early design tip configuration of axial turbines. The second case (Figure 2b) is a conventional squealer tip shape found in most HP turbines of aero-engines and land-based gas turbines. It is characterized by a rim width $w = 1.4\%$ H and a depth $d = 6\%$ H . The third case (Figure 2c) is the GE's shelf design as proposed, where a portion of the PS rim is shifted toward the blade camber line and extends between the blade axial chord length locations $C_{ax} = 0.1$ and $C_{ax} = 0.7$. The last case (Figure 2d) is also a shelf design but with an inclined PS rim by the angle $\theta = 25^\circ$. These four tip configurations were investigated under both stationary and moving shrouds (turbine casing). In the moving case, the rotor remains stationary, whereas the shroud is subjected to motion from the SS to the PS, as depicted by the blue arrow in Figure 2. This assumption was proven effective in examining the relative motion effects similar to rotating blades on the leakage flow and aerodynamic losses at the tip region [11, 26–29].

3 | Computational Method

3.1 | Solver and Turbulence Model

Three-dimensional steady Reynolds-averaged Navier-Stokes (RANS) method was used to evaluate the aerodynamic features of the rotor tips using ANSYS-CFX [30]. It is a computational fluid dynamics (CFD) software based on the finite volume method primarily dedicated to turbomachinery flows. The high-resolution method (second order) was applied for both the advection scheme and turbulence computations. The heat transfer equation is solved using the total energy option. A conservative option is chosen with a time scale factor of 1 for the fluid time scale control. The chosen RANS turbulence model is the SST $k-\omega$ with gamma-theta ($\gamma-Re_\theta$) transition formulation [31, 32]. This model was chosen for its demonstrated suitability in transonic turbine applications [11, 33], as it effectively captures near-wall turbulence, flow separation, and laminar-to-turbulent transition. These features are critical for accurately predicting the aerothermal performance of the turbine blade tips under investigation. In contrast, other RANS models, such as the standard $k-\epsilon$ and $k-\omega$, are less reliable in predicting flows with adverse pressure gradients and separation. While higher-fidelity approaches like large Eddy simulation (LES) offer a detailed resolution of turbulent structures, they are computationally intensive around the blade tip and exceed the requirements of this engineering application. HP

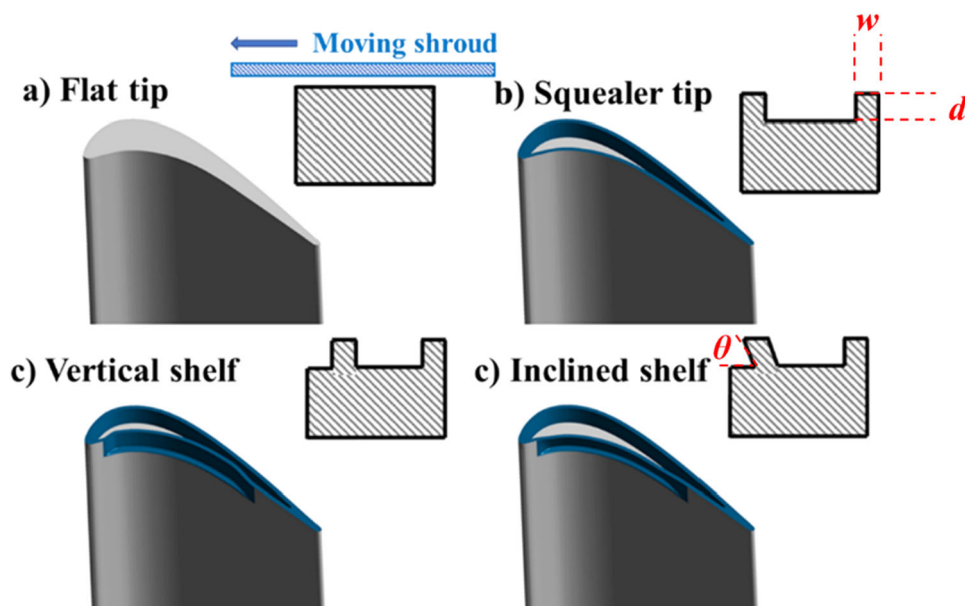


FIGURE 2 | 3D investigated tip configurations with cross section schematic diagrams, and shroud movement representation. [Color figure can be viewed at [wileyonlinelibrary.com](https://onlinelibrary.wiley.com)]

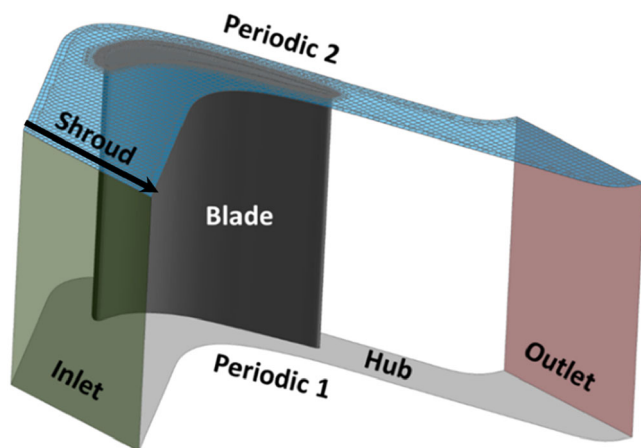


FIGURE 3 | Computational domain and boundary conditions. [Color figure can be viewed at [wileyonlinelibrary.com](https://onlinelibrary.wiley.com)]

turbine blades are most likely subject to boundary layer (BL) transition, and the $\gamma-Re_\theta$ formulation was specifically designed to capture this phenomenon. Various flow convergence criteria were adopted to ensure the computational results are effectively accurate, including plotting the static pressure at both the blade surface and the numerical domain exit and monitoring the root-mean-square (RMS) residuals of the continuity, momentum, turbulent kinetic energy, specific dissipation rate, and energy equations to reach 10^{-5} . Reducing the convergence to 10^{-6} and 10^{-7} has resulted in a negligible error of 0.1% and 0.12%, respectively.

3.2 | Boundary and Operating Conditions

The computational domain and boundary conditions are given in Figure 3. The flow inlet was positioned at one axial chord length from the blade leading edge (LE), while the outlet was positioned at one and a half axial chord from the blade trailing

edge (TE). Two periodic boundaries were imposed in the pitchwise direction to cover only one rotor blade. The boundary conditions were imposed as follows. The domain inlet features a P_0 total pressure with a flow direction angle $\alpha = 27.43^\circ$, a turbulence intensity $I = 4\%$, and a total temperature $T_0 = 432$ K. At the outlet, a static pressure was specified with an averaging option applied across the entire surface. All the walls, including the blade surfaces, hub, and shroud, were considered non-slip walls and isothermal with a static temperature $T_{\text{wall}} = 288$ K. To simulate the relative motion between the rotor blade and the casing, a moving shroud boundary condition was applied. Therefore, the linear speed of the shroud was set to $U_{\text{shroud}} = 410$ m/s on the shroud surface along the pitch direction, as illustrated in Figure 3. This translation speed corresponds to a typical HP turbine rotational speed $\Omega = 10,000$ rpm. This analogy is often adopted in studies looking at shroud motion effects [26–29].

3.3 | Grid Sensitivity Analysis

A mesh convergence study was conducted to ensure sufficient simulation accuracy of the compressible flow through the rotor, particularly the tip region. Three hybrid meshes (structured and unstructured) were generated using Fluent-Meshing, a coarse mesh of 1.2 million points, a medium mesh of 1.6 million points, and a fine mesh of 2.5 million points. The mesh cell size near the tip region is about five times smaller than the mesh cells at the blade surface. The normalized height of the first cell (y^+) near all walls was kept around 1. An example of the coarse mesh is already shown at the shroud (blue surface) in Figure 3.

Isentropic Mach number distributions at the rotor midspan of the flat tip case at design condition are plotted in Figure 4. The results indicate no difference between the three meshes, as they provide the same results on both the blade suction and PSs. All the meshes capture the smooth transition of the flow speed at

the SS from subsonic around the LE to transonic around the TE. A decision on the mesh that should be selected can not be made at this stage as this requires analyzing its sensitivity to a thermal quantity. Heat flux on the blade surface was chosen to additionally assess the mesh sensitivity. Heat flux distributions at the same midspan location are plotted in Figure 5.

It is shown that the blade SS faces a boundary layer (BL) transition from turbulent to laminar between the LE and the

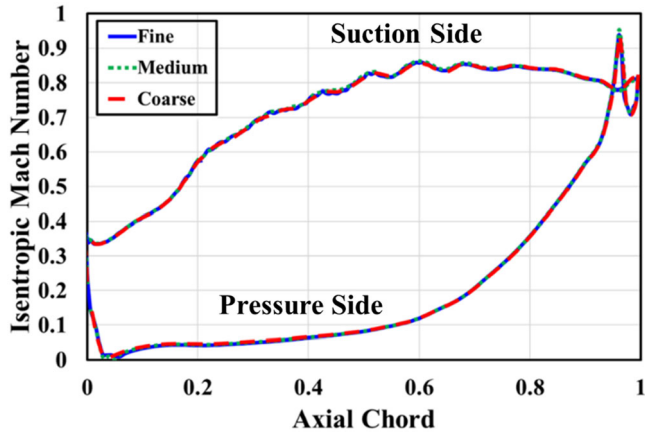


FIGURE 4 | Isentropic Mach number distribution at the midspan for the different grids. [Color figure can be viewed at [wileyonlinelibrary.com](https://onlinelibrary.wiley.com)]

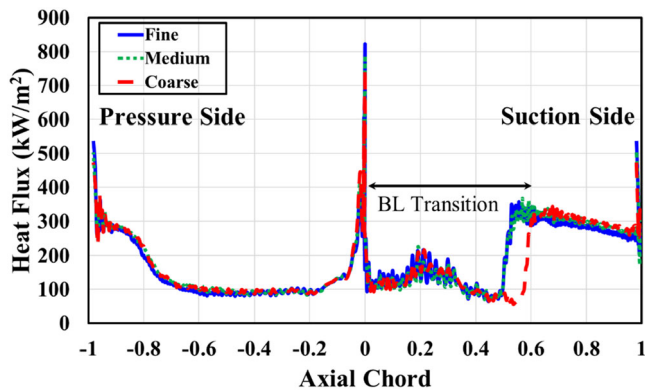


FIGURE 5 | Heat flux distribution at the midspan for the different grids. [Color figure can be viewed at [wileyonlinelibrary.com](https://onlinelibrary.wiley.com)]

mid-chord (i.e., $C_{ax} = 0.5$) region. The coarse mesh predicts a larger transition compared to the medium and fine meshes. Thus, the medium mesh (1.2 million points) was chosen to conduct the simulations in the rest of the study. This mesh offers an independent solution both aerodynamically and thermally compared to the coarse mesh and is more computationally efficient than the fine mesh.

3.4 | Validation With the Experimental Data

Figure 6 presents the comparisons between the current computational solution and experimental data [25] of the isentropic Mach number (M_{is}) at design and off-design conditions. The pressure probes of the measurements from [25] have a constant error of 1%, as shown in the figure. In both cases, design and off-design, the SS flow experiences a rapid acceleration until it reaches a transonic speed at design and a supersonic speed at off-design. At design, the maximum M_{is} is around 0.83 at 0.56 C_{ax} for both the numerical and experimental plots. At off-design, both the experimental and numerical SS flows become supersonic ($M_{is} = 1$) at around 0.58 C_{ax} . After this location, the flow exhibits two peaks due to a shockwave generation at around 0.75 C_{ax} and shock reflection at around 0.94 C_{ax} . The reflection location is well predicted by CFD, but its magnitude is overestimated. At the PS, the simulation predicts the flow in a very good agreement with the experimental data. Overall, the numerical predictions of the Mach number distributions around the rotor surfaces are good at design and good at off-design conditions.

Comparisons of the heat flux distributions at blade midspan are also presented in Figure 7. At the PS, the numerical heat flux performs very well compared to the experimental one at both design and off-design conditions. At this surface of the blade, there are no significant flow features affecting the thermal behavior of the flow as expected. At the blade SS, the BL faces a transition from turbulent to laminar and then back to turbulent. The numerical heat flux magnitude at the transition region is similar to the experimental one. For example, it fluctuates between 110 and 200 kW/m^2 for the design case and it is at around 110 kW/m^2 for the off-design case. However, the transition length is quite similar in the design case but not in the off-design case. The numerical simulation underestimates the length of the transition at off-design, but it provides good

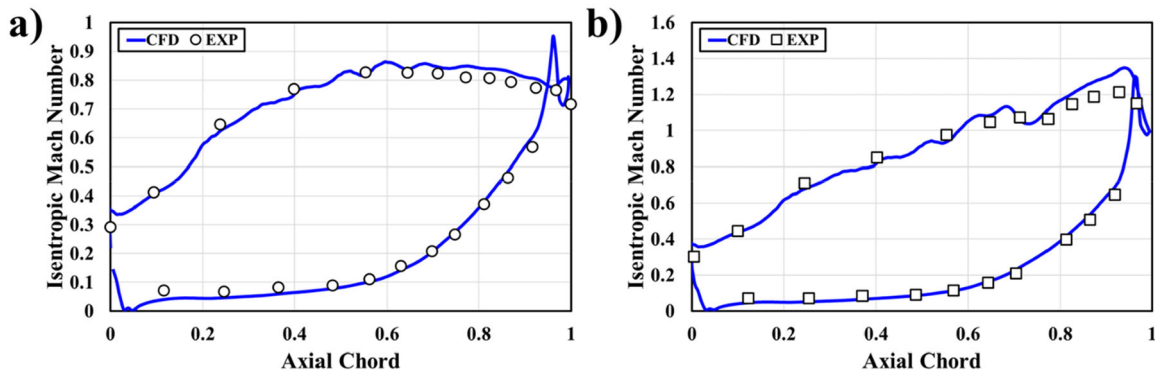


FIGURE 6 | CFD versus experimental data: isentropic Mach number distribution at the blade midspan (a) design case and (b) off-design case. [Color figure can be viewed at [wileyonlinelibrary.com](https://onlinelibrary.wiley.com)]

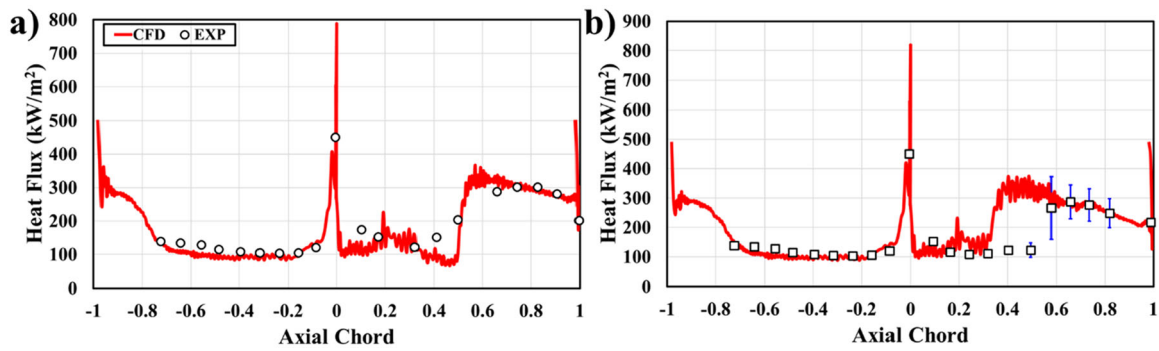


FIGURE 7 | CFD versus experimental data: heat flux distribution at the midspan (a) design case, and (b) off-design case. [Color figure can be viewed at [wileyonlinelibrary.com](https://onlinelibrary.com)]

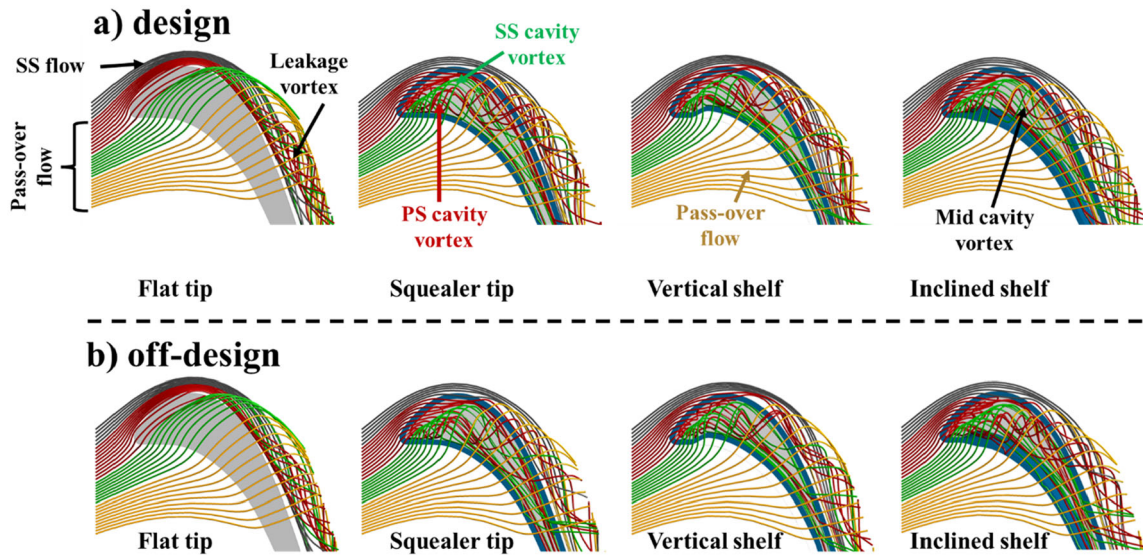


FIGURE 8 | 3D streamlines through the tip clearance (a) design case, and (b) off-design case. [Color figure can be viewed at [wileyonlinelibrary.com](https://onlinelibrary.com)]

agreement with the experimental measurements downstream of this location. Note also that the experiment (Figure 7b) has a large measurement error downstream of the transition location, where the error ranges between 20% (i.e., $0.5 C_{ax}$) and 40% (i.e., $0.657 C_{ax}$). This could be attributed to the reflection of shock waves from the surface where the sensor is mounted. Moreover, some of the discrepancies between the computation and the experiment could be attributed to the use of the default coefficients of the SST γ - Re_θ model [31, 32], which are initially calibrated for subsonic flows. Improved validation of the off-design case (high Mach number flow) can be achieved by model calibration [34, 35]; however, this is out of the scope of this study. Overall, the numerical predictions of the heat flux distributions are good at design and acceptable at off-design conditions.

4 | Results and Discussions

4.1 | Flow Structure Through the Tip Clearance at Stationary Condition

In Figure 8, three-dimensional streamlines were used to visualize the flow structure across the blade tip clearance for the investigated tip configurations (flat tip, squealer, vertical shelf,

and inclined shelf). It is well known that the tip clearance flow has a pressure-driven nature between the blade PS and SS, which causes a complex flow pattern including several secondary vortices [2]. So, the aim of this sub-section is to visualize the complex flow pattern at each configuration. Note that the flow behavior in the design (Figure 8a) and off-design (Figure 8b) cases is quite similar; thus, the discussion in this sub-section is valid for both cases. Four packs of streamlines were highlighted, and they begin upstream of the blade LE at the axial location $C_{ax} = 0.15$ and the height $h = 0.98 H$. Each pack has a different color (gray, red, green, and yellow) for effective tracking of the leakage flow.

For the flat tip case, the green and yellow packs pass over the tip almost in parallel way due to the shroud BL. Some streamlines of the red pack also pass over the tip, and the remaining, along with the gray streamlines, narrow down to pass near the blade SS due to its cambered shape. Downstream, all these streamlines contribute to the formation of the TLV. Thus, the flow across this flat tip can be considered simple.

For cavity-based configurations (i.e., squealer and shelf tips), the leakage flow is complex with similar secondary flow structures. The red and green streamlines hit the LE and enter

the tip cavity to form the SS cavity vortex (SSCV) and PS cavity vortex (PSCV), respectively. These vortices are formed due to the interaction between the shroud BL and the strong pressure gradient at the clearance. The pressure gradient twists the BL to form the SSCV, which is a low-pressure vortex, and the PSCV, which is a high-pressure vortex. A portion of the SSCV leaves the cavity early at around $C_{ax} = 0.4$ toward the outer blade SS to form the inner core of the TLV. The rest of the SSCV merges with the PSCV to form together the mid-cavity vortex (MCV), which travels through the cavity toward the TE. Then, a portion of the MCV leaves the cavity under the pressure difference effect to contribute to the formation of mid core of the TLV. Moreover, the yellow pack of streamlines keeps the same pass-over behavior as in the flat tip case since it passes through the sub-viscous layer of BL of the shroud. Thus, it does not enter the cavity. After crossing the tip clearance, the yellow pack forms the external envelope of the TLV. Furthermore, similar flow complexity has also been found in previous studies [17, 36–39], but with a few differences in terms of size and location. These differences are due to the blade airfoil shape, boundary conditions, and squealer tip dimensions.

4.2 | Flow Structure Inside the Tip Gap at Stationary Condition

Figure 9 reveals the flow structures inside the tip gap at design conditions at three different planes located at 0.2, 0.4, and 0.6 C_{ax} , respectively. Two-dimensional streamlines are used to visualize the flow along with total PR contours representing the pressure loss. The PR is defined as the ratio of the local total pressure to the inlet total pressure. For the flat tip case, the pass-over (leakage) flow is clearly seen parallel to the tip passing from the PS to the SS. Through the chordwise direction, the PR decreases due to the decrease in blade thickness

accompanied by an increase in the leakage amount. The TLV is seen at the 0.4 C_{ax} plane and further increases in size at 0.6 C_{ax} with a high-pressure loss within its core reaching 0.8.

For the cavity-shaped tip cases, the SSCV, PSCV, and MCV vortices are clearly recognized. These vortices induce a high amount of pressure loss, as expected from swirling flows. The highest loss is within the PSCV, which reaches around 0.65 (i.e., at 0.2 C_{ax}). Among these vortices, the SSVC has the smallest size, which is around 2.5 times smaller than that of the PSCV with a relatively higher PR of about 0.82 inside its core. The SSVC is located slightly away from the SS rim wall for the squealer tip and inclined shelf tip, whereas it is in direct contact with the SS rim for the vertical shelf tip. Secondary flows and wall interactions have a significant impact on the heat transfer characteristics at the tip region; it will be discussed later. The MCV forms due to the merge of the twin vortices and dominates the flow patterns inside the cavity to cover the whole cavity width at 0.4 C_{ax} . The MCV size is three times bigger than the PSCV. The minimum value of the PR within the MCV is around 0.69 for all the cavity tips. Note that the TLV is formed early at 0.4 C_{ax} for the vertical shelf case compared to the other two cavity tip cases. This is due to the squeezed cavity width that forces a small amount of the leakage flow to leave the cavity and not contribute to the MCV formation. At the 0.6 C_{ax} plane, the MCV size is considerably contracted since it is sucked out through the SS tip gap to form a major part of the TLV. The minimum pressure loss within the TLV is 0.75, 0.67, and 0.79 for the inclined shelf tip, vertical shelf tip, and squealer tip, respectively. This indicates that the vertical shelf generates the highest loss at this location (i.e., 0.6 C_{ax}), and the inclined shelf performs better than both the vertical shelf and the squealer. However, this result is valid at this local plane only and not found at the domain outlet, where both shelf configurations perform better than the squealer case, as will be shown later. It is worth noting that GE's shelf tip work [24] has shown the presence of the MCV and did not reveal whether other types of cavity secondary flows are present or not.

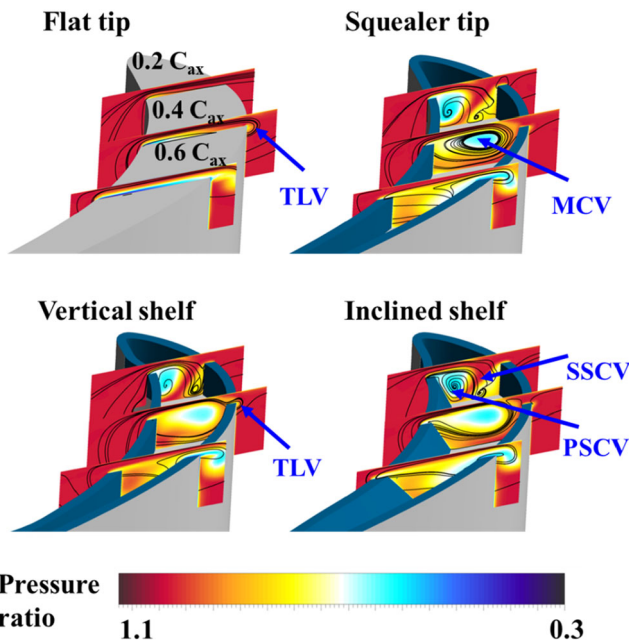


FIGURE 9 | 2D Flow structure at different planes across the tip cavity at design condition and stationary shroud. [Color figure can be viewed at [wileyonlinelibrary.com](https://onlinelibrary.wiley.com)]

4.3 | Design and Off-Design Leakage Flow Rate at Stationary Condition

Reducing the leakage amount is a design goal for highly efficient modern turbines. Increasing over-tip flow reduces the work extracted from the burned gases, leading to higher gas turbine exhaust gas temperatures. Therefore, the over-tip flow is quantified through the SS tip gap outlet surface, colored in red in Figure 10. The area-averaged mass flow rate at this specific location is computed using the following equation:

$$\dot{m}_L = \frac{1}{A} \int \dot{m} dA = \frac{1}{A} \sum_{i=1}^n \dot{m}_i A_i, \quad (1)$$

where \dot{m}_L is the total area tip leakage mass flow rate, A is the total area, \dot{m}_i is the mesh cell mass flow rate, and A_i is the cell area.

Figure 11 presents the leakage mass flow ratio (MFR % inlet), which is the tip leakage mass flow rate \dot{m}_L normalized by the

cascade inlet mass flow rate \dot{m} , for all the geometries at design and off-design conditions. It can be seen that the flat tip case generates the highest leakage under both conditions. In the design condition (Figure 11a), the vertical shelf shows the lowest leakage flow rate, which is 1.21% less than the flat tip MFR. This is due to the squeezed volume of the cavity that led to the early formation of the TLV, as discussed in Figure 9. Moreover, the conventional squealer tip and inclined shelf tip have a 1.11% and 1.01% decrease, respectively, showing that the vertical shelf tip performs the best, followed by the squealer tip.

At the off-design condition (Figure 11b), the MFR trends stay unchanged with regard to the design condition; however, lower leakage values are found. For example, the flat tip leakage has decreased from 14.16% at design to 13.71% at off-design with respect to the inlet mass flow rate, which is a 0.45% decrease. When the exit Mach number increases from subsonic (i.e., $M_{is} = 0.78$) to supersonic (i.e., $M_{is} = 1.1$), a shock wave mechanism develops within the clearance [40], which contributes to the slight reduction in the leakage flow through a slight flow blockage [41]. Regarding the relative change in the MFR, this has also dropped compared to the design case, where it reached -0.79% , -0.87% , and -0.69% for the squealer tip, vertical shelf tip, and inclined shelf tip, respectively, with regard to the flat tip. At stationary conditions, it can be said that the cavity-based tips are able to reduce leakage efficiently at both design and off-design conditions.

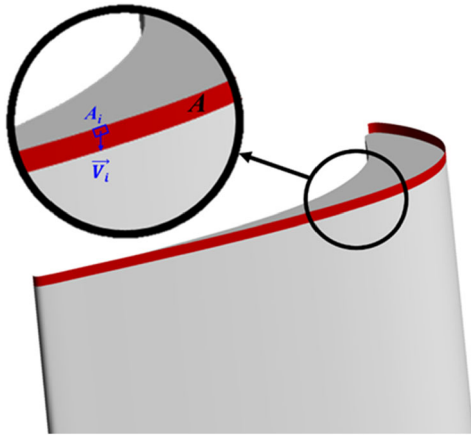


FIGURE 10 | The surface representing the tip clearance exit. [Color figure can be viewed at [wileyonlinelibrary.com](https://onlinelibrary.wiley.com)]

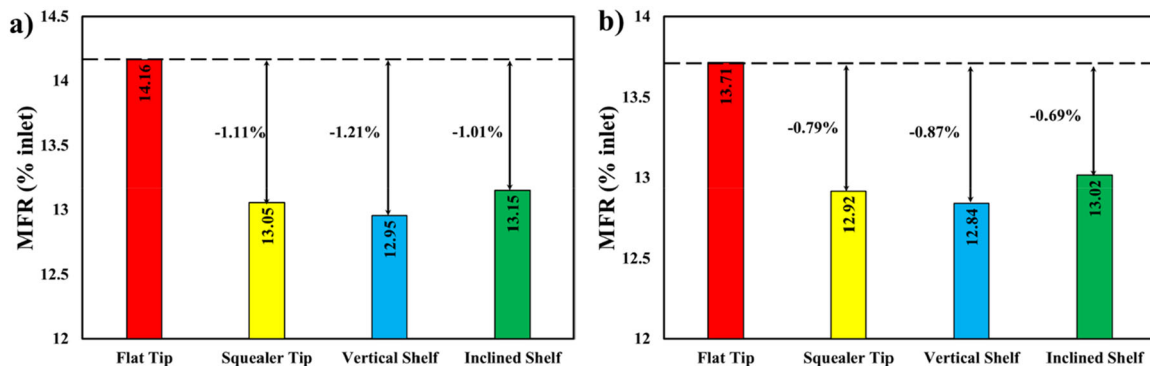


FIGURE 11 | Leakage flow rate ratio at the tip clearance exit (a) design case and (b) off-design case. [Color figure can be viewed at [wileyonlinelibrary.com](https://onlinelibrary.wiley.com)]

4.4 | Design and Off-Design Aerodynamic Losses at Stationary Condition

The aerodynamic performance of rotor blade tips is related to the total pressure loss, sometimes called mixing loss, associated with the TLV that may combine with the high momentum SS passage flow [1, 2]. The total pressure coefficient is used to quantify the effect of different tip structures on the aerodynamic loss of the rotor cascade. The total pressure loss is determined as follows:

$$Y_p = \left(\frac{P_{0,\text{inlet}} - P_{0,\text{outlet}}}{P_{0,\text{inlet}}} \right) \times 100, \quad (2)$$

where $p_{0,\text{inlet}}$ and $p_{0,\text{outlet}}$ are the area-averaged total pressure at the domain inlet and outlet, respectively. The mixing loss (Y_p) for the different tips at design and off-design conditions is plotted in Figure 12. It is clearly seen that the cavity-based tips have the lowest losses compared to the flat tip. This is in agreement with the tip leakage results in Figure 11. Note that the leakage flow rate and pressure loss do not always correlate in accordance with, at some conditions, the low MFR, which may generate very intense TLV that has a high swirl velocity, which leads to a higher mixing loss [11].

At design condition (Figure 12a), the flat tip shows the highest losses with $Y_p = 4.527$, as expected, due to having the narrowest clearance leading to a high pressure loss with the TLV. The shelf-based tips show promising results with more than 6% loss reduction compared to the conventional squealer tip, which has 5.85% less loss with regard to the flat tip. It appears that the shelf design attenuates the sharp pressure gradient between the blade PS and SS by reducing the distance between the rims compared to the squealer design, resulting in lower pressure losses. It is worth noting that the vertical shelf design originally studied by Prakash et al. [24] was found to produce higher aerodynamic loss compared to the conventional squealer design, whereas the inclined shelf design was the most efficient among them. This finding was under rotation conditions and will be later compared with this paper's results under shroud motion.

At the off-design condition (Figure 12b), the total pressure loss trends stay similar to the design condition with the inclined shelf tip outperforming (having the lowest loss) all designs. However, very high losses are generated. The deviation with respect to the design

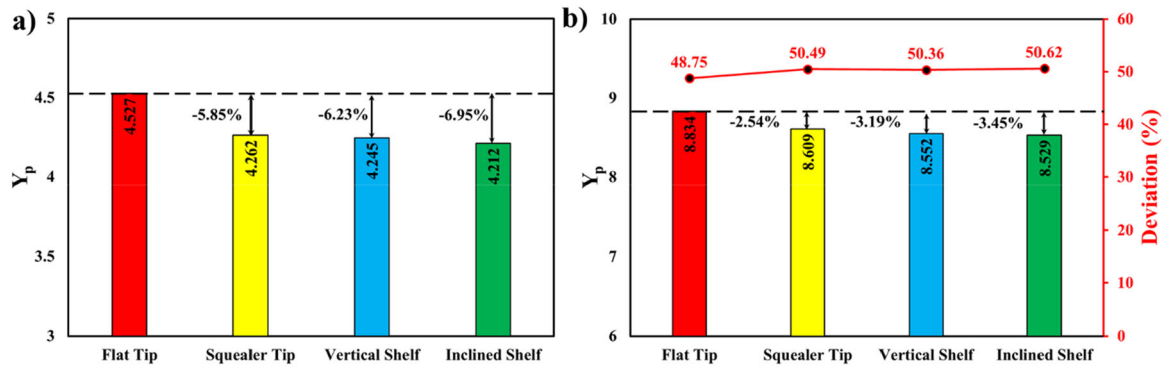


FIGURE 12 | Total pressure loss (a) design case, and (b) off-design case with deviation. [Color figure can be viewed at [wileyonlinelibrary.com](https://onlinelibrary.wiley.com)]

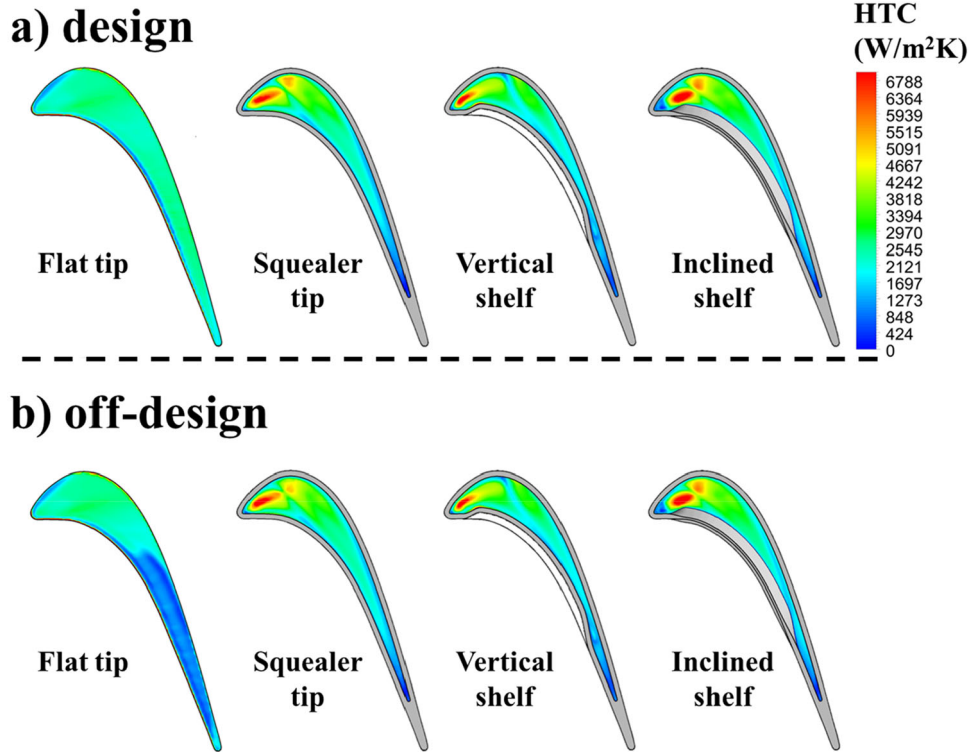


FIGURE 13 | Contours of the heat transfer coefficient at the tip surface (a) design case and (b) off-design case. [Color figure can be viewed at [wileyonlinelibrary.com](https://onlinelibrary.wiley.com)]

case was calculated and added to Figure 12b. The loss is almost doubled when the isentropic Mach number jumps from 0.78 to 1.1, which is a drastic deterioration in the aerodynamic performance. In addition, the relative decrease in the cavity-based tip losses with respect to the flat tip loss has increased by almost half when compared with the design condition. For example, Y_p has raised to -2.54% , -3.19% , and -3.45% for the squealer tip, vertical shelf tip, and inclined shelf tip, respectively. This indicates that none of the tip designs is effective against off-design conditions.

4.5 | Heat Transfer Characteristics of the Tip at Stationary Condition

Rotor tip thermal fatigue is directly related to the heat transfer between the leakage flow and the tip surface. This section offers a detailed analysis of the thermal load on the tip, which is

driven by the leakage flow dynamics for the different tip configurations. Heat transfer maps for the four tip configurations are highlighted in Figure 13 at both design and off-design. The HTC is defined as follows:

$$\text{HTC} = \frac{q}{(T_{\text{flow}} - T_{\text{wall}})}, \quad (3)$$

where q is the heat flux, T_{flow} is the leakage flow temperature near the wall, and T_{wall} is the temperature of the tip surface.

In the used turbulence model, the heat flux is computed by

$$q = \rho c_p u^* \tau_w \quad \text{with} \quad u^* = f(c_\mu, k) \quad \text{and} \quad k = f(\tau_w), \quad (4)$$

where ρ is the fluid density, c_p is the fluid heat capacity, u^* is the flow velocity scale within the logarithmic zone of the BL, c_μ

is the turbulence model constant, and k is the turbulent kinetic energy, which is proportional to the wall shear stress τ_w . Detailed equations of each of these quantities are provided in [30].

At design condition (Figure 13a), it can be noticed that the flat tip configuration has a relatively homogeneous HTC distribution due to the relatively uniform flow across the clearance, where the streamlines were found parallel to the shroud (i.e., Figure 8). A thin strip of low HTC can be seen at the PS, which is due to the flow separation when suddenly changing its direction to cross the tip clearance.

In contrast, the cavity-base tips exhibit high levels of heat transfer in some locations due to the secondary flows present within the cavity. Two high heat transfer spots are identified near the LE of the squealer tip and inclined shelf tip, respectively. These high heat transfer levels are owing to the impingement of the SSCV and PSCV on the tip surface. The small spot corresponds to the SSCV due to its smaller size, whereas the larger spot resulted from the PSCV. This finding shows how the HTC is directly related to the skin friction from the secondary flows. During the impingement, the vortices generate a high wall shear stress τ_w due to their high rotational momentum. The τ_{wall} is directly proportional to k (i.e., Equation 4), so the higher the shear stress, the higher the turbulent kinetic energy. As a result, a significant local surface heat flux increase appears at the vortice spots. The maximum HTC at these spots is around $6800 \text{ W/m}^2 \text{ K}$, which is 52.2% higher than the average HTC value over the tip surface. Note that the vertical shelf tip has only one single high heat transfer spot corresponding to the PSCV. This is because the SSCV was found closer to the SS rim, as discussed earlier (i.e., Figure 9), and thus, the heat transfer at the corresponding tip surface is not significant.

At off-design condition (Figure 13b), the HTC of the flat tip is drastically dropped downstream of the mid-chord location. The reason for this is the significant increase in the flow speed through the clearance to become supersonic. Shockwaves are generated and strongly interact with the flat tip BL, and consequently, the tip surface flow structure is altered. This evidence can be seen in Figure 14, where surface streamlines are compared between the design and off-design cases. At low-speed conditions ($M_{is} = 0.78$), the surface flow features a longer reattachment line (L_{rd}) after a separation (red line) due to the sudden flow direction change from the blade SS to the tip clearance. At high speed ($M_{is} = 1.1$), the shock alters the reattachment line by reducing its length ($L_{ro} < L_{rd}$) and shifting it toward the PS. This interaction induces a larger separation zone promoting a weak BL momentum that translates into a low heat transfer, as found in Zhang et al. [40, 41]. Regarding the cavity-based tip configurations, their HTC distribution at off-design is quite similar to the design condition. High heat transfer spots are present in the same locations. This indicated that the shock mechanism is weakened by the cavity, which agrees with Li et al. [38].

Now the mechanisms (i.e., wall shear stress from secondary flows) responsible for the heat transfer maps of each tip configuration have been revealed; it is important to look at a quantitative analysis of the thermal performance of the studied

tips. This is shown in Figure 15 with the area-average HTC of the tip surfaces at design and off-design. For the flat tip, the HTC exhibits a sharp drop by about 23% from design to off-design showcasing the strong effect of the formed shocks at this region when the blade operates at a transonic Mach number. Comparing the off-design case of the flat tip with the cavity-based tips, the HTC is the worst, with a drop in the ~28% range. This finding suggests that if cooling holes are introduced on the flat tip surface, it is less likely that their cooling will be effective due to the deteriorated heat transfer. Moreover, the HTC of the cavity-based cases at both design and off-design takes close values as it fluctuates between the minimum and maximum values of 2962 and $3032 \text{ W/m}^2 \text{ K}$, which is around a 2.3% change. Note that the vertical shelf tip has the lowest HTC among the cavity-based designs, as expected, which is due to the non-contribution of SSCV in improving the HTC.

4.6 | Flow Structure Through the Tip Clearance at Moving Condition

Figure 16 shows a comparison of the three-dimensional flow structure across the clearance at both stationary and moving shroud cases at the design condition. The flat tip is compared with the squealer tip and the shelf-based designs are not shown due to their similar flow structure to the squealer tip case. The packs of streamlines with the same color codes (gray, red, green, and yellow) from Figure 8 are used for this comparison.

For both the flat tip and squealer tip, it is shown that the shroud motion has caused the streamlines to shift toward the LE. The high speed of the shroud (410 m/s) provides additional momentum to the leakage flow in the LE region, causing local shockwaves that result in increased static pressure and a reduction in leakage flow velocity [11]. The rise in static pressure and drop in flow speed are well-known characteristics of flow downstream of a shockwave. This effect increases the pressure difference between the SS and PS across the clearance, causing streamlines to shift toward the LE. Notably, the shroud's relative motion induces a change in flow conditions, leading the TLV to spin off from the blade SS under these altered conditions. Its swirling behavior has also diminished compared to the design case. This suggests that the pressure loss (Y_p) will decrease as the TLV is the main contributor to this loss. For the squealer tip, most of the red streamlines bypass the clearance under the altered flow conditions, leading the PSCV to form from the green streamlines instead of the red ones. Consequently, the SSCV disappears.

4.7 | Leakage Flow Rate at Moving Condition

Figure 17 examines the MFR (% inlet) under moving shroud condition and also shows the MFR deviation with regard to the stationary condition. Overall, the shroud motion has led to a decrease in the tip leakage flow for the different tip configurations, as expected. It was mentioned that shroud motion induces a shock mechanism that reduces the posterior (downstream the shock) leakage speed, and consequently, the

Design ($M_{is} = 0.78$) Off-design ($M_{is} = 1.1$)

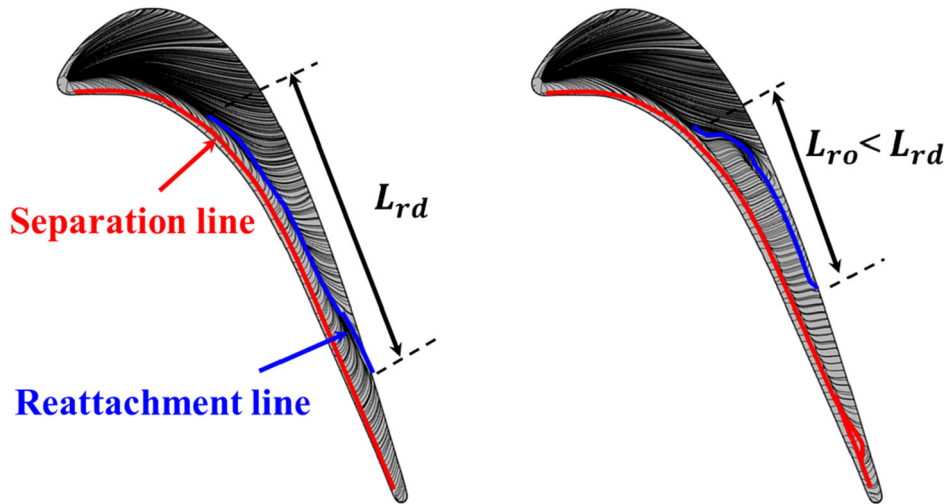


FIGURE 14 | Surface streamlines on the flat tip (a) design case and (b) off-design case. [Color figure can be viewed at [wileyonlinelibrary.com](https://onlinelibrary.wiley.com)]

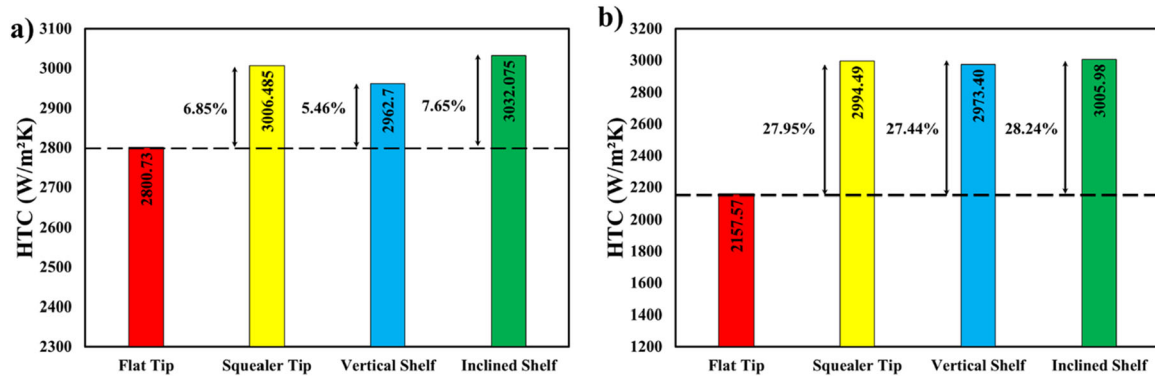


FIGURE 15 | Area-average heat transfer coefficient on the tip surfaces (a) design case, and (b) off-design case. [Color figure can be viewed at [wileyonlinelibrary.com](https://onlinelibrary.wiley.com)]

mass flow rate through the clearance declines. This finding agrees well with Krishnababu et al. [10], Xie et al. [42]. Moreover, the flat tip case generates the lowest leakage under motion conditions, with a 3.35% decline from the stationary case. The cavity presence was found to reduce the effect of the shocks formed under shroud motion and lead to a slightly higher leakage rate than the flat tip case. However, the cavity-based cases generated less leakage compared to the stationary case leakages, with the vertical shelf tip having the lowest MFR of -1.31% , followed by the squealer tip of -1.29% , and then the inclined shelf of -1.23% . These findings exhibit notable differences compared to the results reported for GE's shelf tip in Prakash et al. [24], where the inclined shelf configuration was found to yield the lowest leakage flow rate, followed by the squealer tip and then the vertical shelf. This discrepancy can likely be attributed to several factors, including differences in blade aerofoil geometry, the turbulence models employed, and the operating conditions. Specifically, in Prakash et al. [24], the $k-\epsilon$ turbulence model was used, whereas the present study adopts the SST $k-\omega$ with gamma-theta ($\gamma-Re_\theta$) transition formulation, which is known to provide more accurate predictions of flow separation and BL transition effects. Additionally,

detailed information on the operating conditions, such as PRs, Mach numbers, and thermal loads, was not provided in Reference [24], further contributing to the discrepancy observed between the current findings and those of GE. Back to the present findings, the lowest MFR found in the vertical shelf tip is due to the narrow cavity width compared to the other cavities, which forces the PSCV to suck less leakage and consequently have a smaller size. The inclined shelf tip has a larger PSCV size than both the vertical shelf tip and squealer tip, similar to the stationary case shown in Figure 9.

4.8 | Aerodynamic Losses at Moving Condition

The shroud motion is shown to promote a significant reduction in the cascade mixing loss compared to the mixing loss at stationary conditions, as illustrated by the deviation data in Figure 18. This reduction takes the values of 22.19%, 17.64%, 18.44%, and 14.77% for the flat tip, squealer tip, vertical shelf, and inclined shelf. This loss reduction is mainly due to the spin-off of the TVL away from the blade SS, as shown in Figure 16. Comparing the different configurations under shroud motion, it

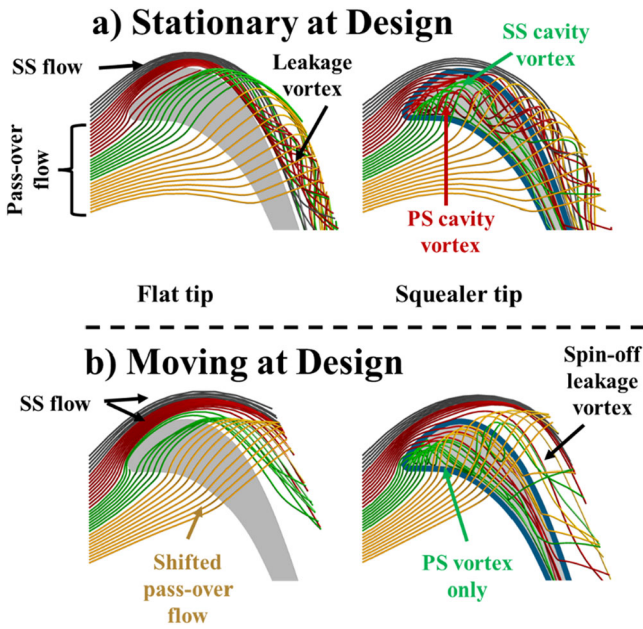


FIGURE 16 | 3D streamlines through the tip clearance (a) stationary shroud at design case and (b) moving shroud at design case. [Color figure can be viewed at [wileyonlinelibrary.com](https://onlinelibrary.wiley.com)]

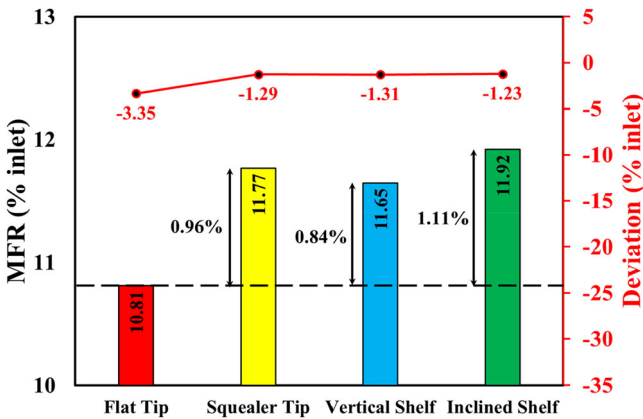


FIGURE 17 | Leakage flow rate ratio at the tip clearance exit under shroud motion. [Color figure can be viewed at [wileyonlinelibrary.com](https://onlinelibrary.wiley.com)]

is shown that all the cavity-based tip configurations are performing better than the flat tip. The vertical shelf tip is showing the lowest loss (-3.37%) followed by the squealer tip (-2.26%) and then the inclined shelf tip (-0.95%) with regard to the flat tip loss. This can be attributed to the less leakage sucked by the PSCV of the vertical shelf tip compared to the squealer tip and inclined shelf tip cases, which both have larger PSCV sizes, thus contributing to more losses. Thus, the vertical shelf can be seen as the best configuration for both lower leakage and lower aerodynamic loss.

4.9 | Heat Transfer Characteristics at Moving Condition

The effect of shroud movement on the HTC is highlighted in Figure 19 using the area-averaged values of the tip surfaces. For the flat tip, the HTC has increased by 2.39% compared to the

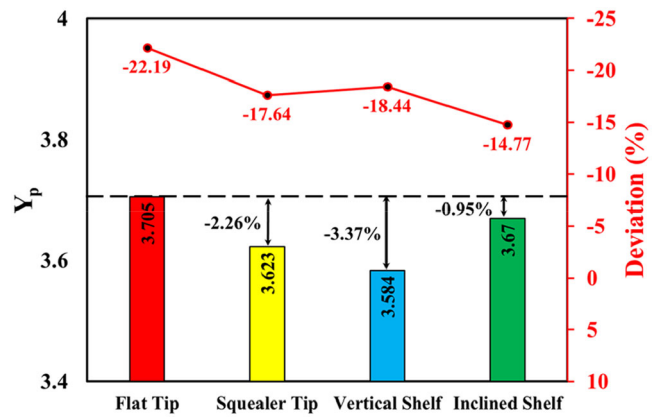


FIGURE 18 | Total pressure loss under shroud motion. [Color figure can be viewed at [wileyonlinelibrary.com](https://onlinelibrary.wiley.com)]

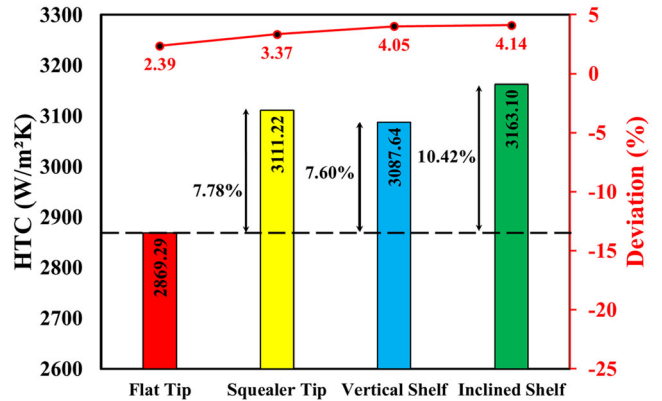


FIGURE 19 | Area-average heat transfer coefficient on the tip surfaces under shroud motion. [Color figure can be viewed at [wileyonlinelibrary.com](https://onlinelibrary.wiley.com)]

stationary case due to the higher wall shear stress induced by the shroud motion.

Cavity-based configurations have higher HTC under shroud motion compared to the flat tip case, as expected, due to the presence of secondary flows. In addition, the emerging secondary flow topology under the motion of the shroud (that was identified by the larger PSCV dominating the LE region on the tip surface, as seen in Figure 16) has contributed to the increase of the HTC compared to the case with stationary shroud. The HTC increased by 3.37%, 4.05%, and 4.14% for the squealer tip, vertical shelf, and inclined shelf, respectively. The large nature of the PSCV contributes to more τ_w applied on the tip surface, which improves the tip surface heat transfer.

It is also shown that the vertical shelf has a lower HTC of $3087.64 W/m^2K$ compared to the squealer tip and inclined shelf, which have HTCs of 3111.22 and $3163.1 W/m^2K$, respectively. This aligns with the pressure loss results (Figure 18), indicating that the smaller PSCV of the vertical shelf produces less loss and, consequently, a lower HTC compared to the larger PSCV of the squealer tip and inclined shelf. Overall, the inclined shelf emerges as the best configuration, having the highest HTC, which is a desirable feature for improved mixing in the clearance if film cooling is applied.

4.10 | Trade-Off Analysis

The performance of the present high-pressure turbine blade tips has been assessed based on three critical parameters: HTC, tip leakage flow rate (MFR), and aerodynamic loss (Y_p). The parameters are ranked from best (1) to worst (4) and plotted in the radar chart in Figure 20. The results are taken from the design case representing cruise condition and under shroud motion simulating the turbine stage rotation. The comparison of the four tip configurations (flat tip, squealer tip, vertical shelf tip, and inclined shelf tip) reveals significant trade-offs in thermal and aerodynamic efficiency. The flat tip, representative of early-generation turbine blades (i.e., from the 1950s), exhibits the lowest tip leakage due to its minimal clearance. However, it also has the lowest HTC and the highest aerodynamic loss, making it thermally inefficient and aerodynamically suboptimal. As a result, this design has been phased out in favor of more advanced configurations. The squealer tip, widely used in the previous generation of turbofans of the 1990s, improved upon the flat tip by increasing HTC and reducing aerodynamic loss. However, it does not perform optimally in leakage control, making it less favorable compared to modern shelf tip designs. The vertical shelf tip patented by GE, which is currently in use in their modern turbofan engines (i.e., GENx), provides a balance between all three-performance metrics. It demonstrates moderate HTC, improved leakage control compared to the squealer tip, and the lowest aerodynamic loss among the four configurations. These attributes contribute to its adoption in current high-pressure turbine designs. The inclined shelf tip, investigated as a potential design improvement, achieves the highest HTC, indicating superior cooling potential as a high HTC allows effective heat dissipation when coupled with internal cooling mechanisms (e.g., film cooling, impingement cooling). However, this comes at the expense of increased tip leakage, which may impact overall efficiency. While its aerodynamic loss is lower than that of the flat tip, it remains higher than that of the vertical shelf tip. This suggests that further optimization of leakage control strategies is required for its practical implementation.

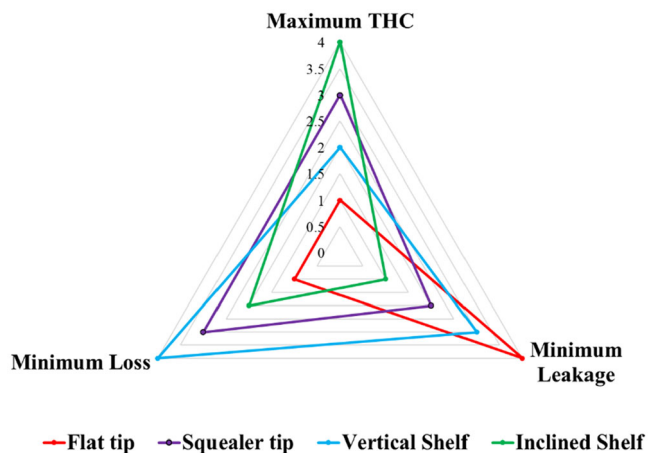


FIGURE 20 | Trade-off chart of the studied blade tip configurations. [Color figure can be viewed at [wileyonlinelibrary.com](https://onlinelibrary.wiley.com)]

5 | Conclusions

This study used CFD to analyze the aerodynamic and thermal characteristics of a modern turbine blade tip, specifically GE's vertical and inclined shelf tips, under both design and off-design transonic conditions. Results were compared to conventional designs, including the flat and squealer tips, with the effect of shroud motion also considered to replicate turbine stage rotation. The numerical method demonstrated good alignment with experimental data, validated through isentropic Mach number and heat flux measurements.

Under stationary shroud conditions, the cavity-based designs showed complex secondary flow structures, including vortex formation within the tip cavity. Due to the strong pressure gradient and interaction with the shroud BL, suction-side and pressure-side cavity vortices (SSCV and PSCV) developed, ultimately forming the TLV responsible for aerodynamic losses. High-speed shroud motion caused streamlines to shift toward the leading edge (LE) due to increased static pressure and reduced flow velocity downstream of shockwaves. This motion also changed flow conditions, leading to the disappearance of the SSCV and causing the TLV to spin off with reduced swirling, which decreased both pressure loss (Y_p) and leakage flow rate.

Among the configurations, the vertical shelf tip demonstrated the lowest tip leakage rate in both stationary and moving conditions, indicating its effectiveness in controlling leakage. It also exhibited low-pressure losses, attributed to its smaller PSCV, although it had a slightly lower HTC with 2.75% ($75.46 \text{ W/m}^2\text{K}$) lower than the inclined shelf and 0.77% ($23.58 \text{ W/m}^2\text{K}$) lower than the squealer tip. The conventional squealer tip showed somewhat higher leakage and pressure losses than the vertical shelf but performed moderately well across test conditions. In contrast, the inclined shelf displayed the highest HTC, which is advantageous for cooling applications, particularly when film cooling is applied, although it had a higher leakage rate and greater mixing losses than the other designs. Interestingly, these results differ from previous findings on GE's shelf tip, where the inclined shelf achieved the lowest leakage rate.

The trade-off analysis findings indicate that while the vertical shelf tip provides a well-balanced design, the inclined shelf tip offers the potential for enhanced cooling efficiency. However, its increased tip leakage requires further optimization to improve overall performance. Future research should focus on evaluating shelf tip designs under more realistic conditions, including the effects of film cooling, full-stage rotation, and unsteady interactions from the combustion chamber. Investigating these factors will provide deeper insights into the aerodynamic and thermal performance of modern turbine blade tips.

Acknowledgments

The authors are thankful to the Algerian Ministry of Higher Education and Scientific Research for their generous support of this project. The authors would like to express their sincere gratitude to Nottingham Trent University for its generous support through open access

publication. We acknowledge the use of AI-based software “Gemini” to assist in polishing the language of the abstract and conclusion sections of this manuscript. The software was employed solely for language refinement to enhance clarity and readability, without altering the scientific content or interpretations. After using this tool, the author reviewed and edited the content as needed and took full responsibility for the content of the publication.

Data Availability Statement

Data that support the findings of this study are available from the corresponding author upon reasonable request.

References

1. R. S. Bunker, “A Review of Turbine Blade Tip Heat Transfer,” *Annals of the New York Academy of Sciences* 934, no. 1 (2001): 64–79.
2. R. S. Bunker, “Axial Turbine Blade Tips: Function, Design, and Durability,” *Journal of Propulsion and Power* 22, no. 2 (2006): 271–285, <https://doi.org/10.2514/1.11818>.
3. R. S. Bunker, “The Augmentation of Internal Blade Tip-Cap Cooling by Arrays of Shaped Pins,” *ASME Journal of Turbomachinery* 130, no. 4 (July 2008): 041007, <https://doi.org/10.1115/1.2812333>.
4. G. S. Azad, J. Han, S. Teng, and R. J. Boyle, “Heat Transfer and Pressure Distributions on a Gas Turbine Blade Tip,” *ASME Journal of Turbomachinery* 122, no. 4 (February 2000): 717–724, <https://doi.org/10.1115/1.1308567>.
5. P. Jin and R. J. Goldstein, “Local Mass and Heat Transfer on a Turbine Blade Tip,” *International Journal of Rotating Machinery* 9, (2003): 159736, <https://doi.org/10.1155/S1023621X03000083>.
6. R. Dong-Ho and H. C. Hyung, “Effect of Vane/Blade Relative Position on Heat Transfer Characteristics in a Stationary Turbine Blade: Part 1- Tip and Shroud,” *International Journal of Thermal Sciences* 47, no. 11 (2008): 1544–1554.
7. R. Dong-Ho and H. C. Hyung, “Effect of Vane/Blade Relative Position on Heat Transfer Characteristics in a Stationary Turbine Blade: Part 2-Blade Surface,” *International Journal of Thermal Sciences* 47, no. 11 (2008): 1528–1543.
8. D. H. Rhee and H. H. Cho, “Effect of Vane/Blade Relative Position on Heat Transfer Characteristics in a Stationary Turbine Blade: Part 2. Blade Surface,” *International Journal of Thermal Sciences* 47 (2008): 1544–1554.
9. N. L. Key and T. Arts, “Comparison of Turbine Tip Leakage Flow for Flat Tip and Squealer Tip Geometries at High-Speed Conditions,” *Journal of Turbomachinery* 128 (2006): 213–220.
10. S. K. Krishnababu, W. N. Dawes, H. P. Hodson, G. D. Lock, J. Hannis, and C. Whitney, “Aerothermal Investigations of Tip Leakage Flow in Axial Flow Turbines—Part II: Effect of Relative Casing Motion,” *ASME Journal of Turbomachinery* 131, no. 1 (2009): 011007.
11. Z. Mansouri, A. Settar, and H. Khamane, “Computational Investigation of Heat Load and Secondary Flows Near Tip Region in a Transonic Turbine Rotor With Moving Shroud,” *Applied Thermal Engineering* 136 (2018): 141–151, <https://doi.org/10.1016/j.applthermaleng.2018.03.012>.
12. G. S. Azad, J. Han, and R. J. Boyle, “Heat Transfer and Flow on the Squealer Tip of a Gas Turbine Blade,” *ASME Journal of Turbomachinery* 122, no. 4 (February 2000): 725–732, <https://doi.org/10.1115/1.1311284>.
13. G. S. Azad, J. Han, R. S. Bunker, and C. P. Lee, “Effect of Squealer Geometry Arrangement on a Gas Turbine Blade Tip Heat Transfer,” *ASME Journal of Heat Transfer* 124, no. 3 (May 2002): 452–459, <https://doi.org/10.1115/1.1471523>.
14. M. El-Ghandour, M. K. Ibrahim, K. Doi, and Y. Nakamura, “Effects of Tip Cavity Depth, Width, and Location on the Leakage Flow in an Axial Turbine Cascade,” *Journal of Fluid Science and Technology* 5, no. 3 (2010): 558–573.
15. B. Mischo, T. Behr, and R. S. Abhari, “Flow Physics and Profiling of Recessed Blade Tips: Impact on Performance and Heat Load,” *ASME Journal of Turbomachinery* 130, no. 2 (February 2008): 021008, <https://doi.org/10.1115/1.2775485>.
16. J. H. Kim, S. Y. Lee, and J. T. Chung, “Numerical Analysis of the Aerodynamic Performance and Heat Transfer of a Transonic Turbine With a Partial Squealer Tip,” *Applied Thermal Engineering* 152 (2019): 878e89.
17. S. Jiang, Z. Li, and J. Li, “Effects of the Squealer Winglet Structures on the Heat Transfer Characteristics and Aerodynamic Performance of Turbine Blade Tip,” *International Journal of Heat and Mass Transfer* 139 (2019): 860e72.
18. N. Lomakin, A. Granovskiy, V. Shchaulov, and J. Szwedowicz, “Effect of Various Tip Clearance Squealer Design on Turbine Stage Efficiency,” in *Proceedings of the ASME Turbo Expo 2015: Turbine Technical Conference and Exposition. Volume 2A: Turbomachinery* (ASME, 2015), V02AT38A017, <https://doi.org/10.1115/GT2015-42726>.
19. Y. Fu, F. Chen, H. Liu, and Y. Song, “Experimental and Numerical Study of Honeycomb Tip on Suppressing Tip Leakage Flow in Turbine Cascade,” *ASME Journal of Turbomachinery* 140, no. 6 (April 2018): 061006, <https://doi.org/10.1115/1.4039049>.
20. H. Ma, Q. Zhang, L. He, Z. Wang, and L. Wang, “Cooling Injection Effect on a Transonic Squealer Tip—Part II: Analysis of Aerothermal Interaction Physics,” *Journal of Engineering for Gas Turbines and Power* 139 (2017): 052507.
21. C. Zhou and F. Zhong, “A Novel Suction-Side Winglet Design Philosophy for Highpressure Turbine Rotor Tips,” *Journal of Turbomachinery* 139, no. 111002 (2017): 1–11.
22. S. W. Lee, J. H. Cheon, and Q. Zhang, “The Effect of Full Coverage Winglets on Tip Leakage Aerodynamics Over the Plane Tip in a Turbine Cascade,” *International Journal of Heat and Fluid Flow* 45 (2014): 23–32.
23. D. G. Cherry, C.-P. Lee, C. Prakash, et al., “Turbine Blade Having Angled Squealertip,” United States Patent, NO USOO6672829B1 (2004), <https://patents.google.com/patent/US6672829B1/en>.
24. C. Prakash, C. P. Lee, D. G. Cherry, R. Doughty, and A. R. Wadia, “Analysis of Some Improved Blade Tip Concepts,” *ASME Journal of Turbomachinery* 128, no. 4 (February 2005): 639–642, <https://doi.org/10.1115/1.2220050>.
25. J. H. Nicholson, A. E. Forest, M. L. G. Oldfield, and D. L. Schultz, “Heat Transfer Optimized Turbine Rotor Blades—An Experimental Study Using Transient Techniques,” in *Proceedings of the ASME 1982 International Gas Turbine Conference and Exhibit. Volume 4: Heat Transfer; Electric Power* (ASME, 1982), V004T09A019.
26. V. Srinivasan and R. J. Goldstein, “Effect of Endwall Motion on Blade Tip Heat Transfer,” *Journal of Turbomachinery* 125, no. 2 (2003): 267–273.
27. T. Yasa, G. Paniagua, and A. Bussolin, “Performance Analysis of a Transonic High-Pressure Turbine,” *Proceedings of the Institution of Mechanical Engineers, Part A: Journal of Power and Energy* 221 (2007): 769–778.
28. Y. Zhang, Y. Liu, Y. Li, and Q. Li, “Numerical Study on Aerothermal Performance of Shroud Movement in the Vivinity of Turbine Tips,” *Thermal Science* 25, no. 5 Part A (2021): 3365–3375.
29. H. Luo, X. Qiang, and B. Zhang, “Research on Turbine Blade Squealer Tip Film Holes Arrangement and Moving Shroud,” *Aerospace Systems* 5, no. 3 (2022): 491–501.
30. “Ansys CFX-Solver Theory Guide,” ANSYS, Inc, 2021.
31. F. R. Menter, R. B. Langtry, S. R. Likki, Y. B. Suzen, P. G. Huang, and S. Völker, “A Correlation Based Transition Model Using Local Variables

Part 1- Model Formulation,” *ASME Journal of Turbomachinery* 128, no. 3 (2006): 413–422.

32. R. B. Langtry, F. R. Menter, S. R. Likki, Y. B. Suzen, P. G. Huang, and S. Völker, “A Correlation Based Transition Model Using Local Variables Part 2 - Test Cases and Industrial Applications,” *ASME Journal of Turbomachinery* 128, no. 3 (2006): 423–434.

33. Z. Mansouri, “Unsteady Simulation of Flow and Heat Transfer in a Transonic Turbine Stage Under Non-Uniform Inlet Conditions,” *International Communications in Heat and Mass Transfer* 129 (2021): 105660, <https://doi.org/10.1016/j.icheatmasstransfer.2021.105660>.

34. P. Malan, K. Suluksna, and E. Juntasaro, “Calibrating the Gamma-Re_theta Transition Model for Commercial CFD,” in *47th AIAA Aerospace Sciences Meeting Including the New Horizons Forum and Aerospace Exposition. 47th AIAA Aerospace Sciences Meeting Including the New Horizons Forum and Aerospace Exposition* (American Institute of Aeronautics and Astronautics, 2009), <https://doi.org/10.2514/6.2009-1142>.

35. S. Mauro, R. Lanzafame, M. Messina, and D. Pirrello, “Transition Turbulence Model Calibration for Wind Turbine Airfoil Characterization Through the Use of a Micro-Genetic Algorithm,” *International Journal of Energy and Environmental Engineering* 8 (2017): 359–374.

36. C. B. Senel, H. Maral, L. A. Kavurmacioglu, and C. Camci, “An Aerothermal Study of the Influence of Squealer Width and Height Near a HP Turbine Blade,” *International Journal of Heat and Mass Transfer* 120 (2018): 18–32.

37. X. Yan, Y. Huang, K. He, J. Li, and Z. Feng, “Numerical Investigations Into the Effect of Squealer–Winglet Blade Tip Modifications on Aerodynamic and Heat Transfer Performance,” *International Journal of Heat and Mass Transfer* 103 (2016): 242–253.

38. L. Li, C. Tu, C. Wang, Y. Sun, J. Zou, and J. Zhang, “Control of the Leakage Flow and Heat Transfer Characteristics at the Blade Tip by Cavity Filling,” *Results in Engineering* 20 (2023): 101446, <https://doi.org/10.1016/j.rineng.2023.101446>.

39. T. Wang and Y. Xuan, “A Novel Approach for Suppressing Leakage Flow Through Turbine Blade Tip Gaps,” *Propulsion and Power Research* 11, no. 4 (2022): 431–443, <https://doi.org/10.1016/j.jprr.2022.08.003>.

40. Q. Zhang and L. He, “Overtip Choking and Its Implications on Turbine Blade-Tip Aerodynamic Performance,” *Journal of Propulsion and Power* 27, no. 5 (2011): 1008–1014, <https://doi.org/10.2514/1.b34112>.

41. Q. Zhang, D. O. O’Dowd, L. He, A. P. S. Wheeler, P. M. Ligrani, and B. C. Y. Cheong, “Overtip Shock Wave Structure and Its Impact on Turbine Blade Tip Heat Transfer,” *Journal of Turbomachinery* 133, no. 4 (2011): 041001, <https://doi.org/10.1115/1.4002949>.

42. W. Xie, X. Peng, H. Jiang, et al., “Experimental Study of Turbine Blade Tip Heat Transfer With High-Speed Relative Casing Motion,” in *Proceedings of Global Power and Propulsion Society* (GPPS-TC-2021–0267, 2021).